Journal of Materials Chemistry A

Unique Li4Ti5O12/TiO2 multilayer arrays with advanced surface lithium storage capability

Journal:	*Journal of Materials Chemistry A*
Manuscript ID	TA-ART-04-2018-003075.R2
Article Type:	Paper
Date Submitted by the Author:	01-Jun-2018
Complete List of Authors:	Ge, Hao; Liaoning University, Shenyang, Cui, Luxia ; Liaoning University, Shenyang Sun, Zhi-Jia; Liaoning University, College of Chemistry Wang, Denghu; Liaoning University, Shenyang Nie, Shengnan; Liaoning University, Shenyang Zhu, Shuai; Liaoning University, Shenyang Matthews, Bryan; University at Buffalo, SUNY, Chemical and Biological Engineering; Wu, Gang; University at Buffalo, SUNY, Chemical and Biological Engineering Song, Xi-Ming; Liaoning Key Laboratory for Green Synthesis and Preparative Chemistry of Advanced Materials, Liaoning University, Ma, Tianyi; University of Newcastle, School of Environmental & Life Sciences

Journal Name

ARTICLE

Unique $Li_4Ti_5O_{12}/TiO_2$ multilayer arrays with advanced surface lithium storage capability

Received 00th January 20xx,
Accepted 00th January 20xx

DOI: 10.1039/x0xx00000x

www.rsc.org/

Hao Ge [a], Luxia Cui [b], Zhijia Sun [a], Denghu Wang [a], Shengnan Nie [a], Shuai Zhu [a], Bryan Matthews [c], Gang Wu *[c], Xi-Ming Song *[a] and Tian-Yi Ma *[d]

Nanostructured arrays grown on metal substrates have been attracting considerable attention as promising electrode materials for energy storage system. Herein, unique $Li_4Ti_5O_{12}/TiO_2$ multilayer arrays (LTO/TiO_2 MLA) featuring advanced surface lithium storage capability are successfully synthesized for the first time via a facile substrate-free hydrothermal method with subsequent calcination. The proposed substrate-free growth mechanism of the LTO/TiO_2 MLA is demonstrated in detail. Compared to previously reported LTO and LTO/TiO_2 arrays grown on various substrates, novel multilayer array structure and remarkable surface lithium storage capability have been clearly detected in our newly prepared LTO/TiO_2 MLA. The unique framework of LTO/TiO_2 MLA can not only offer abundant grain boundaries and phase interfaces for increasing the number of Li^+ storage sites but also provide rich and hierarchical channels to ensure more lithium ions and electrons rapidly diffuse and migrate, contributing to advanced surface lithium storage capability. The as-prepared LTO/TiO_2 MLA exhibit great practical potentials for further achieving both high-capacity and high-rate lithium storage, delivering an ultrahigh reversible capacity of 193 mAh g^{-1} at 0.5 C and a superior rate capability of 148 mAh g^{-1} at 30 C between 1.0 and 2.5 V. Our present work provides a facile yet scalable and substrate-free approach for rational design and fabrication of multilayer arrays with superior electrochemical performance. We believe that the multilayer arrays structure with abundant active sites and diffusion channels will arouse intense interests.

1. Introduction

Rechargeable lithium-ion batteries (LIBs) have been widely used in our modern life due to their high energy density and cycle longevity.[1-4] However, current LIBs still cannot fulfill the demand of certain energy storage applications, such as, power electric vehicles, including hybrid electric vehicles (HEVs), plug-in hybrid electric vehicles (PHEVs), and pure electric vehicles (EVs).[5-7] Conventional LIBs using graphite as the anode active material generally suffer from a short high rate cycle life, and have some serious safety concerns; Such as, the formation of highly reactive dendritic lithium on the anode surface, especially during high rate discharging, which may easily penetrate through, or grow around, the porous separator and thereby cause an internal short circuit.[8] Therefore, there is a demand to develop alternative anode materials with improved safety, cycling stability, and rate performance for power LIBs. Spinel $Li_4Ti_5O_{12}$ (LTO) is a promising carbon-free anode active material that has attracted considerable attention.[9-13] It possesses a lithium insertion/extraction voltage of approximately 1.55 V (*vs.* Li^+/Li), which avoids the reduction of the electrolyte on the electrode surface and the formation of the solid electrolyte interphase (SEI) layer, thus offering excellent safety. Furthermore, LTO exhibits a zero-volume change and high thermal stability during the lithium intercalation/deintercalation processes, ensuring outstanding cycle stability. Unfortunately, low theoretical capacity (175 mAh g^{-1}) and inferior reaction kinetics, originating from poor electrical conductivity and a low lithium-ion diffusion coefficient, impede its potential application for high-power LIBs.[14-17] Thorough attempts have been made to improve the electrochemical performance of LTO, such as nanostructure fabrication, morphological optimization, surface coating, chemical doping, or a combination of aforementioned strategies.[5, 10, 18-20] Promisingly, TiO_2, as a carbon-free material with high theoretical capacity (336 mAh g^{-1}) and superior lithium-ion diffusibility, has been undoubtedly proven to be an outstanding anode additive to augment the reversible capacity and rate performance of LTO.[21-24] Thereafter, a wide range of LTO/TiO_2 composites have been spontaneously demonstrated

[a] Liaoning Key Laboratory for Green Synthesis and Preparative Chemistry of Advanced Materials, College of Chemistry, Liaoning University, Shenyang, 110036, P. R. China. E-mail: songlab@lnu.edu.cn (X. M. Song)

[b] Department of Chemistry and Biochemistry, Graduate School of Engineering, Kyushu University, Fukuoka 819-0395, Japan

[c] Department of Chemical and Biological Engineering, University at Buffalo, The State University of New York, Buffalo, NY, 14260, United States. E-mail: gangwu@buffalo.edu (G. Wu)

[d] Discipline of Chemistry, University of Newcastle, Callaghan, NSW 2308, Australia.. E-mail:tianyi.ma@newcastle.edu.au (T. Y. Ma)

†Electronic Supplementary Information (ESI) available: [details of any supplementary information available should be included here]. See DOI: 10.1039/x0xx00000x

with superior electrochemical performance over bare LTO electrodes.[25-30]

In addition, it is worth noting that the three-dimensional (3D) nanosheet array electrode materials have aroused considerable interest in enhancing the rate performance for LIBs. These arrays have a large exposed effective surface, which offer shortened lithium-ion diffusion paths, improved electron transfer capability, more lithium-insertion channels, and higher contact area between the electrolyte and active materials.[18, 31] Recently, self-supported LTO and LTO/TiO_2 nanosheet arrays grown directly on substrates as 3D anode electrodes, have been reported to demonstrate excellent charge-discharge properties. For example, LTO nanosheet arrays, with vertically aligned rectangular nanosheets of 14 nm in thickness, were successfully synthesized through a hydrothermal treatment of Ti foil in LiOH solution, followed by a calcination process.[32] These possess outstanding rate and cycling capability with a reversible capacity of 163 mAh g^{-1} at 20 C and a capacity retention of 124 mAh g^{-1} after 3000 cycles at 50 C. Porous LTO/TiO_2 nanosheet arrays were constructed by a hydrothermal synthesis process,[18] exhibiting a high initial discharge capacity of 184.6 mAh g^{-1} and excellent electrochemical stability. Additionally, rutile TiO_2 decorated hierarchical $Li_4Ti_5O_{12}$ nanosheet arrays have been reported for lithium ion hybrid supercapacitor applications.[31] The self-supported $Li_4Ti_5O_{12}$-rutile TiO_2 nanosheet arrays possessed a kind of hierarchical 3D interconnected nanostructure with efficient lithium diffusion along the [011] direction of $Li_4Ti_5O_{12}$ and [001] of rutile TiO_2, showing the outstanding energy storage performance. Also, the black mesoporous $Li_4Ti_5O_{12-\delta}$ nanowall arrays, with oxygen vacancies, were successfully synthesized, which greatly improved electrode kinetics, rate performance, and cycling stability, making them a promising 3D anode for advanced lithium-ion microbatteries.[33] However, all the reported LTO and LTO/TiO_2-based nanosheet arrays on metal substrates involve the use of a variety of solvents and relatively sophisticated processes. For instance, generally, Ti foil substrates have to be treated in advance using ethanol, acetone and deionized water. Then, to obtain the precursors, the substrates must undergo a hydrothermal reaction with a NaOH solution, followed by, immersing the substrates in a diluted HCl solution or hydrochloric acid for ion exchange between Na^+ and H^+. Finally, the precursors are immersed into a LiOH solution and go through a hydrothermal and annealing treatment to obtain the resultant samples.[18, 31, 33] Additionally, the growth of LTO and LTO/TiO_2 nanosheet arrays on the substrate is strongly restricted by complicated strategy and reaction conditions, resulting in a rather small loading of active material on the electrode (~ 0.04 mg cm^{-2}), and consequently limiting the areal capacity for the LIB anode (theoretically ~7 μA h cm^{-2}).[32] The challenge remains to synthesize high-performance 3D LTO nanosheet array electrode materials, with alternative fabrication technologies, in order to increase the active material loading of nanosheet arrays for practical application. To the best of our knowledge, there is still no report on the substrate-free preparation of LTO and LTO/TiO_2 arrays.

Bearing in mind the above issues needed to be alleviated, we developed a facile substrate-free hydrothermal strategy of in-situ growth of unique LTO/TiO_2 multilayer arrays (LTO/TiO_2 MLA). Compared to previous reported LTO or LTO/TiO_2 arrays grown on substrates,[18, 31, 32] our newly synthesized LTO/TiO_2 MLA exhibited advanced surface lithium storage capability and improved electrochemical performances for LIBs. The detailed formation and improved mechanism of the LTO/TiO_2 MLA are systematically studied in this paper.

2. Experimental details

2.1 Synthesis of LTO and LTO/TiO_2 MLA

Typically, 0.322 g of $LiOH·H_2O$ was dissolved into 80 ml of deionized water and then 3.3 ml of tetra-n-butyl titanate $Ti(OC_4H_9)_4$ (A.R.) was slowly added into the above solution. After magnetically stirring for 12 h to form a homogeneous suspension, the mixture was transferred to a 100 mL Teflon-lined stainless autoclave and was heated to 130 °C for 16 h. Subsequently, the powders deposited at the bottom of the reactor were collected by centrifuging and washing with ethanol five times. Then, to remove the remaining solvents and yield a precursor, the obtained powders were vacuum dried at 80 °C for 6 h. Finally, the precursor was calcined at 500 °C for 2 h under atmospheric air to obtain the resulting LTO/TiO_2 MLA. Pristine LTO MLA were also synthesized using the same method as mentioned above, however, the molar ratio of Li:Ti was adjusted from 4:5 to 4.5:5.

2.2 Instrumentation

The crystal structures of the obtained samples were characterized by X-ray diffraction (XRD) performed on a Bruker D8 Advance diffractometer (Germany) with monochromatic Cu $K\alpha_1$ (40 kV, 30 mA) radiation at a step size of 0.02° in the range of 5-90°. Scanning electron microscopy (SEM, Hitachi SU8000 series) was performed to investigate the morphologies of as-synthesized materials. The microstructures of the as-prepared powders were further examined with a transmission electron microscopy (TEM, JEM-2100) operating at 200 kV. Nitrogen adsorption-desorption measurements at 77 K were performed using a Micromeritics ASAP 2010 instrument to measure Brunauer-Emmett-Teller (BET) surface areas and porous structures. The pore size distribution was calculated from the adsorption branch of the isotherms using the Barret-Joyner-Halenda (BJH) method.

Electrochemical measurements were carried out using CR2032 coin cells in which lithium metal was used as the counter and reference electrode. The working electrode was prepared by homogeneously mixing the active material, acetylene black and polyvinylidene fluoride (PVDF) binder with a weight ratio of 8:1:1 in N-methyl pyrrolidinone (NMP) solvent and coated onto a copper foil at 10 MPa. The electrodes were cut into disks typically with a diameter of 12 mm and vacuum dried at 120 °C for 24 h. The cell assembly was completed in a glove box filled with pure argon. The electrolyte contained 1 M $LiPF_6$ in a 1:1:1 volume mixture of ethylene carbonate (EC), propylene carbonate (PC) and diethyl

carbonate (DEC). The galvanostatic charge-discharge experiments were conducted using a battery test system (Land CT 2001A, Wuhan, China) at various current densities between 1.0 and 2.5 V *vs.* Li^+/Li at 25 °C. Cyclic voltammetry (CV) curves and electrochemical impedance spectra (EIS) were measured on a CHI660E electrochemical workstation. CV curves were produced at various scanning rates: 0.2, 0.4, 0.8, 1.6, and 2.0 mV s^{-1} between 1.0 and 2.5 V. EIS measurements were performed from 100 kHz to 0.01Hz with alternating voltage amplitude of 5mV.

3. Results and discussion

The overall substrate-free synthesis procedure for the LTO/TiO_2 MLA is depicted in **Fig. 1**. LTO/TiO_2 MLA were derived from the layered structure of the $Li_{1.81}H_{0.19}Ti_2O_5{\cdot}xH_2O$ material (denoted as the precursor) after calcination treatment in atmospheric air. Differing from other reported LTO and LTO/TiO_2 arrays grown on substrates,[18, 31, 32] the obtained LTO/TiO_2 MLA demonstrate the unique structure of multilayer array stacking. Abundant grain boundaries and phase interfaces in this special framework can not only significantly increase the number of Li^+ storage sites but also facilitate Li^+ transfer.[23] Furthermore, rich and hierarchical channels in the unique framework can enable full exposure of the active materials to electrolyte and ensure more lithium ions and electrons rapidly diffuse and migrate. These advantages giving rise to promoted kinetic property of lithium ions and electrons diffusion as well as advanced surface lithium storage capability can effectively enhance the specific capacity and high rate capability of the anode material during charge-discharge processes. Moreover, this stacking structure largely increases the loading of the active material, improving the areal capacity for the LIBs anode.

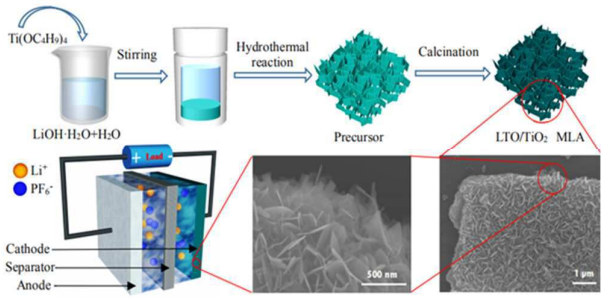

Fig. 1. Fabrication procedure of LTO/TiO_2 MLA without substrate in this study.

3.1 Morphology and structure

The crystalline structure and nano-morphology of the precursors obtained, by adjusting the molar ratio of Li:Ti from 4:5 to 4.5:5 during the substrate-free hydrothermal process at 130 °C for 16 h, are similar (**Fig. 2 and Fig. S1**). From X-ray diffraction (XRD) analysis, all the diffraction peaks for the precursors of LTO/TiO_2 and LTO MLA can be well indexed to orthorhombic $Li_{1.81}H_{0.19}Ti_2O_5{\cdot}xH_2O$ (**Fig. 2a and Fig. S1a**). No other unidentified signals are observed, indicating that the precursors synthesized are highly pure. SEM images clearly show the structure of the arrays: vertically aligned nanosheets with widths ranging between 200 and 300 nm (**Fig. 2b and Fig. S1b**). The corresponding TEM images, shown in **Fig. 2c and Fig. S1c**, further confirm that all of the nanosheets are vertically aligned to form independent arrays with single deck. These nanosheets show uniform thickness of ~10 nm. The high-resolution TEM images (**Fig. 2d and Fig. S1d**) of a single spread nanosheet, illustrate an observable lattice spacing of about 0.83 nm, which matches well with the (200) planes of orthorhombic $Li_{1.81}H_{0.19}Ti_2O_5{\cdot}xH_2O$.[32]

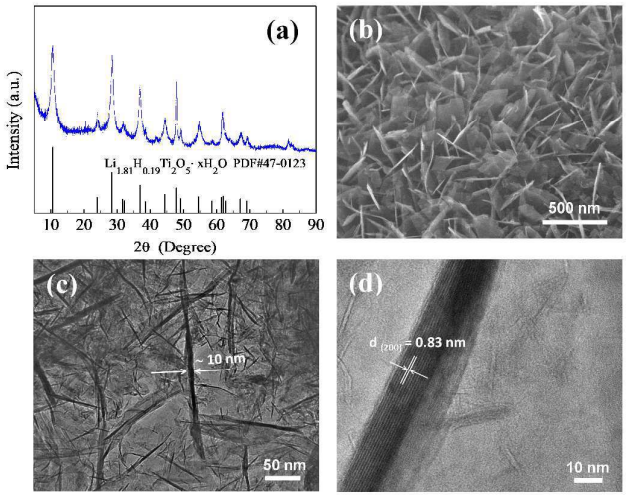

Fig. 2. XRD pattern (a), SEM image (b), TEM (c) and HRTEM image (d) of the precursor $Li_{1.81}H_{0.19}Ti_2O_5{\cdot}xH_2O$ before transforming into LTO/TiO_2 MLA product.

The layered $Li_{1.81}H_{0.19}Ti_2O_5{\cdot}xH_2O$, as a kind of layered hydrous lithium titanate, can be transformed into spinel LTO by a facile heat treatment. **Fig. 3a** and **Fig. S2a** highlight the XRD patterns of LTO/TiO_2 and LTO MLA converted by their corresponding precursors after calcination, indicating that all specimens are well crystallized. All of the well-defined diffraction peaks observed from LTO/TiO_2 and LTO MLA can be indexed to cubic spinel LTO (JPCDS card no. 49-0207), suggesting that the layered hydrous lithium titanate, $Li_{1.81}H_{0.19}Ti_2O_5{\cdot}xH_2O$, has been transformed into spinel LTO. Although the theoretical molar ratio of Li:Ti in spinel $Li_4Ti_5O_{12}$ is 4:5, the Li source will slightly volatilize during the calcination process. Therefore, the pristine LTO is formed when the reactant ratio of Li source:Ti source is 4.5:5. Meanwhile, when the reactant ratio of Li source:Ti source is 4:5 under the same synthesis condition, the LTO/TiO_2 composite can be obtained due to the excess amount of titanium source. Compared with LTO MLA (**Fig. S2a**), additional diffraction peaks at 25.3°, 37.8°, 48.1°, 54.0° and 55.2°, can be clearly observed in LTO/TiO_2 MLA; these attribute to the (101)、(004)、(200)、(105) and (211) facets of anatase TiO_2 (JCPDS card no. 21-1272), confirming that the lower molar ratio of Li and Ti contributes to the formation of TiO_2.[34] It is widely believed that the introduction of TiO_2 can improve the rate capability and reversible capacity of LTO for LIB applications. The SEM images

of LTO/TiO_2 and LTO MLA show that the 3D structures of vertically, well-aligned, nanosheet arrays are well preserved after calcination (**Fig. 3b and Fig. S2b**). This is highly desirable for the materials' electrochemical applications because anode materials with a 3D MLA structure, generally benefit from significantly shortened transport lengths for both lithium ions and electrons, and thereby possessing enhanced rate capability. Through TEM, a thickness of ~10 nm is estimated for typical vertical nanosheets of LTO/TiO_2 and LTO MLA (**Fig. 3c and Fig. S2c**). Being different from LTO MLA (**Fig. S2d**), LTO/TiO_2 MLA, as seen from a HRTEM image (**Fig. 3d**), offer distinct lattice fringes of 0.48 and 0.35 nm, attributing to the (111) and (101) interplanar spacings of LTO and anatase TiO_2, respectively. These HRTEM results (consistent with the XRD analysis) verify the formation of well-crystallized and closely coupled LTO and TiO_2 domains in LTO/TiO_2 MLA (**Fig. 3a**). Moreover, as seen in the HRTEM image (**Fig. 3d**), there are abundant grain boundaries detected, which can act as channels for lithium-ion transportation.[18, 23]

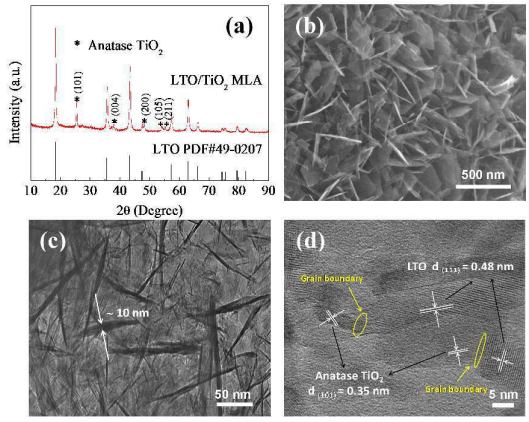

Fig. 3. XRD pattern (a), SEM image (b), TEM (c) and HRTEM image (d) of LTO/TiO_2 MLA.

BET measurements were taken to further characterize the structure of LTO/TiO_2 and LTO MLA stacked by well-interconnected ultrathin nanosheets. The typical IV type adsorption-desorption isotherms can be identified according to the IUPAC classification (**Fig. S3**),[35, 36] showing a distinct hysteresis in the range of ca. 0.5-1.0 P/P_0, indicating the presence of an accessible mesoporous structure.[37] Generally, the mesoporous structure (**Fig. 3b, c and Fig. S2b, c**) formed by closely interconnected standing ultrathin nanosheets, can provide efficient transport pathways for Li^+ and e^- to interior voids and increase the electrode-electrolyte interfacial area. Further, it is worth noting that the specific surface area of LTO/TiO_2 MLA (227.86 $m^2\ g^{-1}$) is larger than that of LTO MLA (196.39 $m^2\ g^{-1}$), while the average pore size of LTO/TiO_2 MLA (~5 nm) is smaller than that of LTO MLA (~10 nm). These results confirm that the modification of TiO_2 can make the surface of LTO/TiO_2 MLA rough (see **Fig. 3d**). Due to the obviously enhanced specific surface area and decreased pore size after modification by TiO_2, the rough surface of LTO/TiO_2 MLA consisting of LTO and TiO_2 should have abundant grain boundaries and phase interfaces. The larger specific surface area and smaller pore size of LTO/TiO_2 MLA, induced by the introduction of TiO_2 on the surface of the LTO nanosheets (see **Fig. 3d**), can offer more active sites for Li^+ insertion, thus reducing electrode polarization and enhancing the utilization efficiency of active materials.

3.2 Formation mechanism

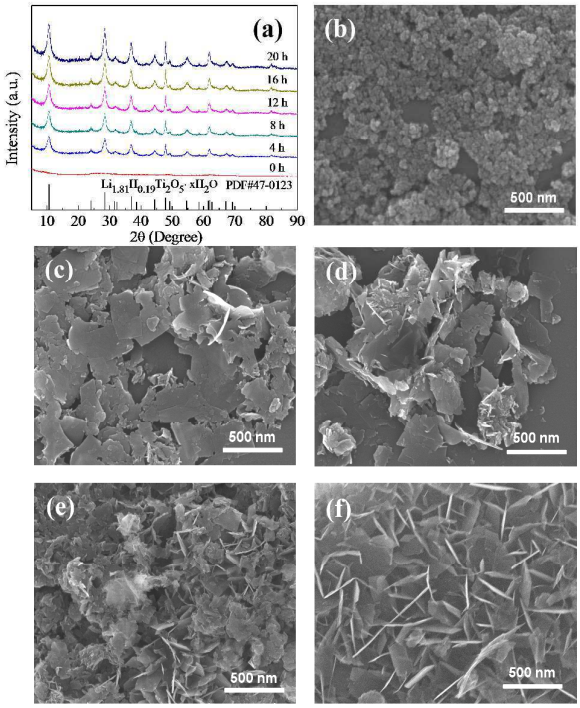

Fig. 4. XRD patterns (a) and SEM images (b-f) of the precursors obtained with different hydrothermal times: (b) 0 h, (c) 4 h, (d) 8 h, (e) 12 h, and (f) 20 h.

Since our reported LTO/TiO_2 MLA present the first 3D, well-aligned, multilayer array structure that is synthesized without a substrate, it is critical to get an insight into its formation mechanism.The actual evolution process of $Li_{1.81}H_{0.19}Ti_2O_5{\cdot}xH_2O$ MLA was explored by examining the time-dependent crystal structure and morphology of the precursors (**Fig. 4**). Before the hydrothermal treatment, amorphous nanoparticle aggregates have already formed (**Fig. 4a and Fig. 4b**). After the hydrothermal treatment, the reactants are completely transformed into the layered $Li_{1.81}H_{0.19}Ti_2O_5{\cdot}xH_2O$ phase without any impurities. The precursors obtained from various reaction times are all layered $Li_{1.81}H_{0.19}Ti_2O_5{\cdot}xH_2O$, however, the typical XRD peaks are gradually intensified with increasing hydrothermal reaction time. Additionally, noticeable differences can be observed from the sequential images of the precursors treated at different times (**Fig. 4b-f, Fig. 2b**). With a 4 h reaction time, nanoparticle aggregates are

first transformed into spreading irregular layers (**Fig. 4b, c**). When the reaction time is increased to 8 h, decreased layer thickness is observed, leading to smaller irregular nanosheets (**Fig. 4d**). Extending the reaction time to 12 h, array structures surrounded by disordered smaller nanosheets are clearly observed (**Fig. 4e**). Finally, well-aligned nanosheet arrays are formed when the hydrothermal reaction time was prolonged to 16 h (**Fig. 2b**). The size and thickness of the self-standing nanosheets clearly increase when the hydrothermal reaction time was further extended from 16 h to 20 h (**Fig. 4f**). Therefore, aforementioned observations revealed the morphological evolution from nanoparticles to nanosheets to uniform nanosheet arrays.

Moreover, hydrothermal temperature and concentration all have significant influence on the materials' morphology. Morphology of the precursors synthesized for 16 h at different temperature were studied. As exhibited in **Fig. S4**, ill-defined nanosheets arrays structure can be formed when temperature is increased from 70 ℃ to 100 ℃. The sample of 130 ℃ displays the most well-developed nanosheets arrays structure (**Fig. 2b**). When temperature reaches 160 ℃, the thickness of the nanosheets increases obviously. At 190 ℃, the precursor appears as aggregates of smaller and thicker nanosheets. Morphology of the precursors synthesized for 16 h at different concentration were also investigated. At lower concentration of 0.01 M (**Fig. S5a**), only small and irregular nanosheets are formed. When the concentration is 0.05 M, the hydrothermal product with nanosheets arrays structure is preliminarily formed (**Fig. S5b**). The well-aligned nanosheets arrays with 300~400 nm in width and ~10 nm in thickness are further obtained at a $LiOH{\cdot}H_2O$ concentration of 0.10 M (**Fig. 2b**). However, at relatively higher concentration of 0.16 M and 0.32 M (**Fig. S5c and d**), serious aggregation has been observed.

Accordingly, the formation mechanism of LTO/TiO_2 MLA via the substrate-free hydrothermal process is proposed as follows. Initially, tetra-n-butyl titanate (TBT) is immediately hydrolyzed by adding it dropwise to an aqueous solution of LiOH, thus producing amorphous hydrous titanium oxide nanoparticles. Similar to Ti foil, the hydrolysate yielded from the hydrothermal treatment, plays significant roles as both the titanium source and the substrate in this system.[31-33] During the hydrothermal treatment process, the soluble Ti^{4+}, from the amorphous hydrous titanium oxide, can react with the Li^+ and OH^- ions to form $Li_{1.81}H_{0.19}Ti_2O_5{\cdot}xH_2O$ nanosheet arrays. The growth process of the nanosheet arrays depends on the dissolution kinetics of the hydrolysate. At the initial stage of the dissolution reaction, irregular $Li_{1.81}H_{0.19}Ti_2O_5{\cdot}xH_2O$ nanosheets are grown. Because the irregular and disordered nanosheets have higher surface energy than well-aligned nanosheets arrays, the irregular precursors tend to be spontaneous self-organization of regularized arrays structure to improve the thermodynamic stability of the system when subjected to long hydrothermal time.[38-40] Consequently, the formed nanosheets dissolve into the solution and gradually developed into smaller nanosheets to construct an array structure through the Ostwald ripening process[41] as the dissolution reaction time progressed. Ultimately, the calcination of the $Li_{1.81}H_{0.19}Ti_2O_5{\cdot}xH_2O$ nanosheet arrays produce LTO/TiO_2 nanosheet arrays.

3.3 Electrochemical performance

To gain an insight into the electrochemical performance of the as-prepared electrodes, the galvanostatic charge-discharge measurements were employed to explore the kinetic processes at different current rates from 0.5 C to 30 C in the potential window of 1.0-2.5 V *vs.* Li^+/Li (**Fig. 5a and b**). Long and flat charge-discharge plateaus around 1.55 V are detected from both LTO and LTO/TiO_2 MLA electrodes, and correspond to the lithiation/delithiation reaction of spinel LTO. Moreover, a short charge-discharge plateau at around 2.00 V/1.75 V can be observed from the LTO/TiO_2 MLA at low rates (0.5 C and 1 C), which is ascribed to the phase transformation from TiO_2 to Li_xTiO_2. However, with increasing current rates, the charge-discharge voltage plateaus of TiO_2 become ill-defined due to the polarization and unsaturated insertion/extrusion of Li^+.[25] Compared with LTO MLA, the LTO/TiO_2 MLA exhibit elongated charge and discharge plateaus, demonstrating a higher utilization efficiency and lower electrode polarization. Notably, LTO/TiO_2 MLA display an ultrahigh discharge capacity of 193.2 mA h g^{-1} at 0.5 C and a superior rate performance of 147.6 mA h g^{-1} at 30 C between 1.0 and 2.5 V vs. Li^+/Li; These values for pure LTO MLA are 173.9 and 92.1 mA h g^{-1} at the same rates, respectively. Therefore, the reversible capacity and rate performance of LTO MLA can be significantly improved after being modified by TiO_2.

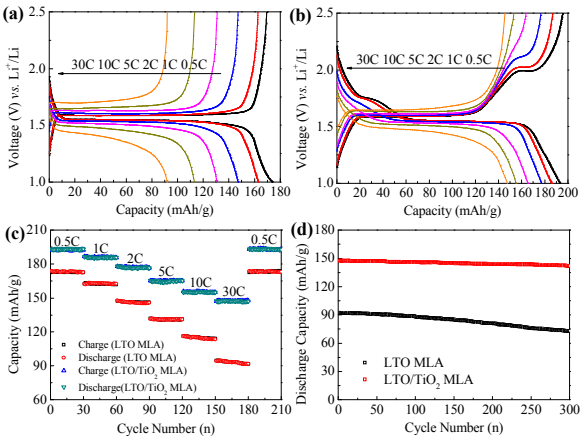

Fig. 5 The galvanostatic charge-discharge voltage profiles of pristine LTO (a) and LTO/TiO_2 MLA (b). Rate capabilities of pristine LTO and LTO/TiO_2 MLA at different rates from 0.5 to 30 C (c). The long-term cycling performances of pristine LTO and LTO/TiO_2 MLA at 30 C for 300 cycles (d).

The rate performances of pristine LTO and LTO/TiO_2 MLA at different current densities were characterized to further confirm the enhanced rate capability of LTO/TiO_2 MLA (**Fig. 5c**). Compared with LTO MLA, the capacity degradation of LTO/TiO_2 MLA is much alleviated upon increasing current density. The capacity retention of LTO/TiO_2 MLA is about 76.4

% at 30 C *vs.* 0.5 C, while LTO MLA is only about 53.0 %. When the current density is returned to 0.5 C after cycling at various rates, the cells have complete capacity recovery, which suggests the excellent cycling stability of LTO and LTO/TiO_2 MLA. The long-term cycling performances of pristine LTO and LTO/TiO_2 MLA at 30 C are displayed in **Fig. 5d**. The LTO/TiO_2 MLA deliver higher capacity of 141.5 mAh g^{-1} after 300 cycles with slight capacity decay during the cycling. However, the value is only 72.6 mAh g^{-1} for pristine LTO MLA. Moreover, the capacity retention ratio of 95.9 % after 300 cycles for LTO/TiO_2 MLA as compared with the initial capacity at 30 C, which is obviously higher than that of pristine LTO MLA (78.8 %), indicates its extremely superior cycle stability and excellent high rate performance. These results confirm that the modification of TiO_2 greatly enhances the cycle performance, especially at high current density. The detailed comparisons of LTO/TiO_2 MLA with previously reported state-of-the-art LTO/TiO_2 arrays further reveal the improved reversible capacity and rate performance of our synthesized composite anodes for power LIBs (**Table 1**).

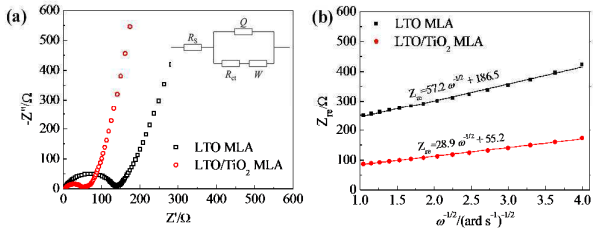

Fig. 6 Electrochemical impedance spectra of pristine LTO and LTO/TiO_2 MLA (a). Graphs of Z_{re} plotted against $\omega^{-1/2}$ at a low-frequency region for pristine LTO and LTO/TiO_2 MLA (b).

The excellent electrochemical performance of the synthesized LTO/TiO_2 MLA anode materials can be attributed to both the unique multilayer array structure and the TiO_2 incorporation. To further study the promoting effect of TiO_2 incorporation on the kinetics of electrode process, electrochemical impedance spectroscopy (EIS) was performed (**Fig. 6**). Typically, both the Nyquist plots of pristine LTO and LTO/TiO_2 MLA consist of a pair of depressed semicircles in high-middle frequency regions, and inclined lines at the low frequency (**Fig. 6a**). An equivalent circuit model (the inset) is employed to analyze the EIS data, in which R_s is the resistance of the electrolyte, and R_{ct} represents the charge-transfer resistance at the electrode/electrolyte interface. The fitting parameters extracted from the Nyquist plots of pristine LTO and LTO/TiO_2 MLA, on the basis of the corresponding equivalent circuit, are shown in **Table 2**. R_s values normally reflect the series resistance (resistance of the electrolyte, separator and electrodes). As compared to LTO MLA, LTO/TiO_2 MLA exhibit a smaller R_s value of 4.3 Ω, which indicates that LTO/TiO_2 MLA possess improved electron conductivity. The major contributor to the charge-transfer resistance (R_{ct}) is the overall resistance of the electrode, which is evaluated to be 87.6 and 32.0 Ω for the pristine LTO and LTO/TiO_2 MLA, respectively. As revealed by the calculated lithium-ion diffusion coefficients (**Table 2**), LTO/TiO_2 MLA display a lithium-ion diffusion coefficient of 9.37×10^{-13} cm^2 s^{-1}, which is a surprising increase in comparison with that of LTO (2.39×10^{-13} cm^2 s^{-1}). The following equations are used to calculate these values: [44, 45]

$$Z_{re} = R_{ct} + R_s + \sigma\omega^{-1/2} \quad (1)$$

$$D_{Li} = \frac{R^2T^2}{2A^2n^4F^4C_{Li}^2\sigma^2} \quad (2)$$

where σ denotes the Warburg impedance factor based on the slopes of the lines in the graph of Z_{re} vs. $\omega^{-1/2}$ (**Fig. 6b**), ω denotes the angular frequency in the low-frequency region, R denotes the gas constant, T denotes the absolute temperature, n denotes the number of electrons transferred in the half-reaction for the redox couple, F denotes the Faraday's constant, A denotes the surface area of the electrode, and C_{Li} denotes the molar concentration of Li^+. From equation (2), increasing the lithium-ion diffusion coefficient and electron conductivity, decreases the charge-transfer resistance. Analyzing for LTO/TiO_2 MLA confirms the promoted reaction kinetics induced by TiO_2 incorporation.

Table 1. Comparison of cycling and rate performances of LTO/TiO_2 MLA with other LTO/TiO_2 arrays reported recently.

Samples	Capacity (mAh g^{-1})					Retention (%)			
	1 C	2 C	5 C	10 C	30 C	2 C	5 C	10 C	30 C
LTO/TiO_2 MLA[a]	186.1	179.5	167.2	156.3	147.8	96.2	89.8	83.9	79.6
LTO/Rutile TiO_2 NSA[31]	185.2	--	158.3	150.8	142.9	--	85.4	81.1	77.2
Porous LTO-TiO_2 NSA[18]	184.3	150.1	125.6	103.2	--	81.3	67.7	55.7	--
Mesoporous-LTO/TiO_2[42]	161.3	152.8	143.5	130.6	--	94..9	88.8	80.7	--
LTO-TiO_2 NWA[24]	150.6	142.3	135.5	129.4	115.5	94.7	90.3	86.3	77.0
LTO/TiO_2 Lamellas[43]	178.5	--	--	154.9	142.3	--	--	82.8	78.7

a: Present work; MLA: Multilayer arrays; NSA : Nanosheet arrays; NWA: Nanowire arrays

Table 2. Fitted Results from EIS.

Samples	LTO MLA	LTO/TiO_2 MLA
R_s/Ω	4.5	3.3
R_{ct}/Ω	87.6	32.0
$D_{Li}/cm^2\ s^{-1}$	2.39×10^{-13}	9.37×10^{-13}

A kinetics analysis (Cyclic voltammetry) was undertaken to supplementary demonstrate the lithium storage behavior of LTO/TiO_2 MLA (**Fig. 7**). The larger oxidation and reduction peak areas of LTO/TiO_2 MLA, especially seen at high scan rates, confirm that LTO/TiO_2 MLA have higher specific capacities than those of LTO MLA at various current rates. The redox peaks of LTO and LTO/TiO_2 MLA at approximately 1.5/1.7 V is assigned to the two-phase reaction between spinel structure of $Li_4T_5O_{12}$ and rock-salt structure of $Li_7T_5O_{12}$.[44] Compared to LTO MLA, extra pairs of redox peaks of LTO/TiO_2 MLA, located around 1.71 V and 2.10 V, are observed, which indicates the existence of the anatase TiO_2 phase in the composite.[23] More interestingly, a splitting cathodic peak is detected in CVs, at every scan rate tested, of LTO/TiO_2 MLA. It is well-known that the relationship between peak currents and scan rates is closely associated with various electrochemical reaction characteristics, including solid phase diffusion-controlled or surface-confined charge-transfer processes.[46-48] In the insert of **Fig. 7**, a linear relationship between the peak current (i) and the square root of the scan rate ($v^{1/2}$) is exhibited for the cathodic peaks of LTO MLA (**Fig. 7a**) and cathodic peaks at higher potentials of LTO/TiO_2 MLA (**Fig. 7b**), revealing a classical diffusion-controlled reaction mechanism. The pseudocapacitive effect is presented according to the linear relationship between the peak current and scan rate for the lower potential peaks in the cathodic process of LTO/TiO_2 MLA, indicating that the electrode reaction of the LTO/TiO_2 MLA is controlled by a mixed process of diffusion-limited reaction and surface-confined charge-transfer processes.[46, 49] Generally, surface lithium storage reaction is a quick lithium-ion insertion process, yielding an extra capacity and improved rate performance.[47, 49] As shown in **Fig. 7b**, the cathodic peak areas at lower potentials of LTO/TiO_2 MLA greatly increase the total areas of cathodic peaks especially at high scan rates. The contribution from the capacitive effect and diffusion-controlled charge can be quantitatively characterized according to the following relationship:[50-52]

$$i = k_1 v + k_2 v^{1/2} \quad (3)$$

Enhanced surface lithium storage (capacitive effect) with increasing scan rate is normally proceeded for insertion-desertion mechanism anode. **Fig. 8a** compares the contribution of capacitive effect and diffusion-controlled charge between the LTO/TiO_2 and LTO MLA. As shown in **Fig. 8a**, the capacitive effect contribution of LTO/TiO_2 MLA is always higher than that of LTO MLA at each scan rate. With the scan rate increasing, the differences of the capacitive effect contribution between the LTO/TiO_2 and LTO MLA become more and more large. These results affirm that LTO/TiO_2 MLA electrode possess advanced surface lithium storage capability. There should be more active sites for the lithium storage on the surface of LTO/TiO_2 MLA than on LTO MLA. The detected increased active sites on the surface further verify that there are abundant grain boundaries and phase interfaces on the surface of LTO/TiO_2 MLA.

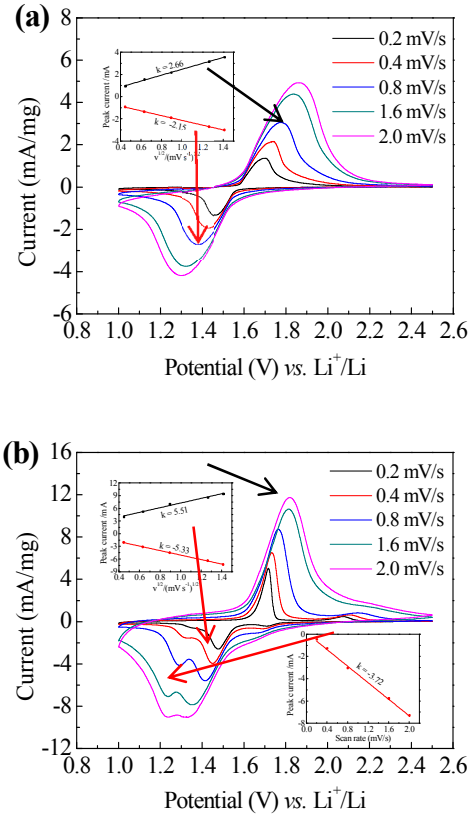

Fig. 7 Cyclic voltammograms of pristine LTO (a) and LTO/TiO_2 MLA (b) at different scan rates between 1.0 and 2.5 V.LTO/TiO_2 MLA

It should be noted that the LTO/TiO_2 and LTO MLA display obvious polarization with enhanced scan rates (**Fig. 7**). This phenomenon can also be observed from the charge-discharge curves (**Fig. 5a and b**). Generally, the potential difference between the anodic and cathodic peaks can reflect the polarization degree of the electrode.[53] However, the splitting cathodic peaks of LTO/TiO_2 MLA make it difficult to compare the polarization degree between LTO/TiO_2 and LTO MLA electrode according to the CV results. Consequently, the polarization of ΔE versus rate plots driven from the charge-discharge curves are employed to discuss the detailed polarization mechanism of the LTO/TiO_2 and LTO MLA. The value of ΔE is defined as the difference between the potentials of charge plateaus and discharge plateaus, which represents

the degree of electrode polarization.[34, 48] As displayed in **Fig. 8b**, the ΔE value of LTO/TiO_2 MLA are smaller than those of pristine LTO MLA at various rates from 0.5 to 30 C, revealing that LTO/TiO_2 MLA has lower electrode polarization and better reaction kinetics. At low current rates (corresponding to low scan rates), both LTO/TiO_2 and LTO MLA exhibit little electrode polarization due to the long transportation time for lithium-ions and electrons. With the current rates increasing, the transportation time for lithium-ions and electrons is decreased, thus leading to obvious electrode polarization. However, the difference value of ΔE between LTO/TiO_2 and LTO MLA becomes more and more large with the current rates enhancing. Obviously, advanced surface lithium storage of LTO/TiO_2 electrode induced by TiO_2 modification is beneficial to reduce electrode polarization, especially at higher current rates (corresponding to high scan rates). These systematical kinetics analysis afford solid evidence that the advanced surface lithium storage process is responsible for the remarkable improvement in reversible capacity and high rate performance of the LTO/TiO_2 MLA anode. Extra lithium storage in grain boundaries and phase interfaces, as well as, lower charge-transfer resistance induced by the synergistic effect between TiO_2 incorporation and well-aligned MLA structure, result in the promoted reaction kinetics and advanced surface lithium storage capability of LTO/TiO_2 MLA.

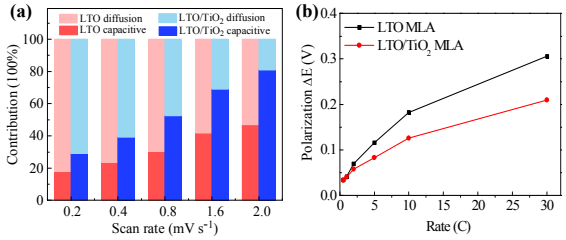

Fig. 8 Normalized contribution ratio of capacitive and diffusion-controlled capacities at different scan rates for pristine LTO and LTO/TiO_2 MLA (a). The polarization of ΔE versus rate plots of pristine LTO and LTO/TiO_2 MLA (b).

It is worth noting that surface manipulation demonstrates important influence on the rate performances of LTO/TiO_2 MLA. Yang *et al*. have reported well-defined $Li_4Ti_5O_{12}$/TiO_2 nanosheet and nanotube composites synthesized by a solvothermal process.[44] Although our work and the mentioned paper[44] all study the morphology and electrochemical performances of $Li_4Ti_5O_{12}$/TiO_2 composites, there are two significant differences between the two works. (1) Surface morphology: Our work reports $Li_4Ti_5O_{12}$/TiO_2 multilayer arrays, whereas the mentioned paper exhibits $Li_4Ti_5O_{12}$/TiO_2 nanosheet and nanotube composites. This difference can be attributed to the different synthesis process employed in the two works. (2) Electrochemical performance: Different from the reported $Li_4Ti_5O_{12}$/TiO_2 nanosheet and nanotube composites, our newly prepared $Li_4Ti_5O_{12}$/TiO_2 multilayer arrays display remarkable surface lithium storage capability. Different morphology of the two composites contributes to this difference. **Fig. 9** compares the rate capabilities of samples driven from precursors of different hydrothermal times and different ratios of the Li:Ti at varied current rates. As exhibited in **Fig. 9a** and **Table S1**, the well-aligned LTO/TiO_2 MLA driven from the precursor of 16 h show the best rate performance. We have also tried more different ratios of the Li:Ti (such as 3.8:5; 3.5:5). Because the concentration of OH^- has markedly influence on the morphology of the precursors (**Fig. S5**), the percentage of the vertically aligned nanosheets tends to be decreased when the ratio of Li:Ti is low (**Fig. S6**). It is supposed that low OH^- concentration can result in the stack of nanosheets. Transforming from stacked nanosheets to well-aligned nanosheets arrays, the effective area and utilization efficiency of the electrode materials will be enhanced, thus leading to high reversible capacity and excellent rate retention. The electrochemical results indicate that LTO/TiO_2 MLA with Li/Ti=4:5 has superior performance at all current rates (**Fig. 9b** and **Table S2**). These results reveal that well-aligned and regularized arrays morphology can effectively enhance the reversible capacity and rate performance of electrode materials. We believe that well-aligned LTO/TiO_2 MLA with ultrahigh reversible capacity and super rate performance have a great practical application value in both the power and energy storage systems.

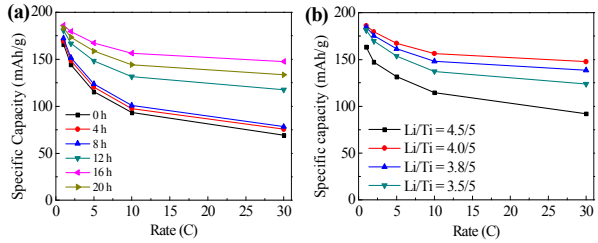

Fig. 9 Rate capabilities of samples driven from precursors of different hydrothermal times (a) and different ratios of the Li:Ti (b) at varied current rates from 1 to 30 C.

Conclusions

In summary, we demonstrate that the unique $Li_4Ti_5O_{12}$/TiO_2 multilayer arrays (LTO/TiO_2 MLA) display advanced surface lithium storage capability. For the first time, a facile substrate-free hydrothermal approach to synthesize LTO/TiO_2 MLA was developed in our work. Four advantages of LTO/TiO_2 MLA collectively contribute to the ultrahigh reversible capacity and superior rate performance: (i) Rich and hierarchical channels in the multilayer array structures can offer large contact area between active materials and the electrolyte, and significantly facilitate the transfer of lithium ions and electrons; (ii)

Abundant grain boundaries and phase interfaces in the framework of LTO/TiO_2 MLA can not only increase the number of Li^+ storage sites but also facilitate Li^+ transfer; (iii) Ultrathin nanosheets greatly shorten the insertion distance of lithium ions and electrons; (iv) Advanced surface lithium storage capability remarkably improves the reversible capacity and rate performance. This work may open new opportunities for large-scale fabrication of multilayer arrays electrode materials with superior electrochemical performance for energy storage system. We anticipate that developing multilayer arrays with advanced surface storage capabilities would be a novel and effective strategy to improve reversible capacity and rate performance for high-power applications.

Acknowledgements

This work was financially supported by the National Natural Science Foundation of China (51108455, 51773085, 21203082, 51273087), Scientific Research Program Foundation of Liaoning Province Education Administration (L2015195), and Australian Research Council (ARC) Discovery Early Career Researcher Award (DE150101306) and Linkage Project (LP160100927). G.W. acknowledge the support from National Science Foundation (CBET-1511528) along with the Sustainable Manufacturing and Advanced Robotics Technology (SMART) Community of Excellence program at the University at Buffalo, SUNY.

Notes and references

1 G.-N. Zhu, Y.-G. Wang and Y.-Y. Xia, *Energy Environ. Sci.*, 2012, **5**, 6652.
2 Y. Tang, Y. Zhang, W. Li, B. Ma and X. Chen, *Chem. Soc. Rev.*, 2015, **44**, 5926.
3 M. V. Reddy, G. V. Subba Rao and B. V. Chowdari, *Chem. Rev.*, 2013, **113**, 5364.
4 L. Lu, X. Han, J. Li, J. Hua and M. Ouyang, *J. Power Sources*, 2013, **226**, 272.
5 B. Zhao, R. Ran, M. Liu and Z. Shao, *Mat. Sci. Eng. R*, 2015, **98**, 1.
6 T.-F. Yi, S.-Y. Yang and Y. Xie, *J. Mater. Chem. A*, 2015, **3**, 5750.
7 J. Ma, C. Wang and S. Wroblewski, *J. Power Sources*, 2007, **164**, 849.
8 N. Nitta, F. Wu, J. T. Lee and G. Yushin, *Mater. Today*, 2015, **18**, 252.
9 H. Zou, X. Liang, X. Feng and H. Xiang, *ACS Appl. Mater. Interfaces*, 2016, **8**, 21407.
10 X. Feng, H. Zou, H. Xiang, X. Guo, T. Zhou, Y. Wu, W. Xu, P. Yan, C. Wang, J. G. Zhang and Y. Yu, *ACS Appl. Mater. Interfaces*, 2016, **8**, 16718.
11 S. D. Kim, K. Rana and J.-H. Ahn, *J. Mater. Chem. A*, 2016, **4**, 19197.
12 Y. Cai, Y. Huang, W. Jia, Y. Zhang, X. Wang, Y. Guo, D. Jia, W. Pang, Z. Guo and L. Wang, *J. Mater. Chem. A*, 2016, **4**, 17782.
13 E. F. Rodriguez, F. Xia, D. Chen, A. F. Hollenkamp and R. A. Caruso, *J. Mater. Chem. A*, 2016, **4**, 7772.
14 X. Lu, L. Gu, Y. S. Hu, H. C. Chiu, H. Li, G. P. Demopoulos and L. Chen, *J. Am. Chem. Soc.*, 2015, **137**, 1581.
15 S. Mao, X. Huang, J. Chang, S. Cui, G. Zhou and J. Chen, *NPG Asia Mater.*, 2015, **7**, e224.
16 X. Wang, D. Liu, Q. Weng, J. Liu, Q. Liang and C. Zhang, *NPG Asia Mater.*, 2015, **7**, e171.
17 L. Peng, H. Zhang, L. Fang, Y. Zhang and Y. Wang, *Nanoscale*, 2016, **8**, 2030.
18 L. Gao, S. Li, D. Huang, Y. Shen and M. Wang, *J. Mater. Chem. A*, 2015, **3**, 10107.
19 S. Wang, Y. Yang, W. Quan, Y. Hong, Z. Zhang, Z. Tang and J. Li, *Nano Energy*, 2017, **32**, 294.
20 X. Li, M. Qu and Z. Yu, *J. Alloys Compd.*, 2009, **487**, L12.
21 T. Song and U. Paik, *J. Mater. Chem. A*, 2016, **4**, 14.
22 S. Ding, J. S. Chen, D. Luan, F. Y. Boey, S. Madhavi and X. W. Lou, *Chem. Commun.*, 2011, **47**, 5780.
23 M. M. Rahman, J.-Z. Wang, M. F. Hassan, D. Wexler and H. K. Liu, *Adv. Energy Mater.*, 2011, **1**, 212.
24 J.-Y. Liao, V. Chabot, M. Gu, C. Wang, X. Xiao and Z. Chen, *Nano Energy*, 2014, **9**, 383.
25 F. Wu, X. Li, Z. Wang and H. Guo, *Nanoscale*, 2013, **5**, 6936.
26 J. Guo, W. Zuo, Y. Cai, S. Chen, S. Zhang and J. Liu, *J. Mater. Chem. A*, 2015, **3**, 4938.
27 L. Gao, L. Wang, S. Dai, M. Cao, Z. Zhong, Y. Shen and M. Wang, *J. Power Sources*, 2017, **344**, 223.
28 C.-T. Hsieh, I. L. Chen, Y.-R. Jiang and J.-Y. Lin, *Solid State Ionics*, 2011, **201**, 60.
29 S. Wang, Y. Yang, C. Jiang, Y. Hong, W. Quan, Z. Zhang and Z. Tang, *J. Mater. Chem. A*, 2016, **4**, 12714.
30 Y. Xia, B. Sun, Y. Wei, B. Tao and Y. Zhao, *J. Alloys Compd.*, 2017, **705**, 58.
31 L. Gao, D. Huang, Y. Shen and M. Wang, *J. Mater. Chem. A*, 2015, **3**, 23570.
32 S. Chen, Y. Xin, Y. Zhou, Y. Ma, H. Zhou and L. Qi, *Energy Environ. Sci.*, 2014, **7**, 1924.
33 Q. Xia, N. Jabeen, S. V. Savilov, S. M. Aldoshin and H. Xia, *J. Mater. Chem. A*, 2016, **4**, 17543.
34 Y. Q. Wang, L. Gu, Y. G. Guo, H. Li, X. Q. He, S. Tsukimoto, Y. Ikuhara and L. J. Wan, *J. Am. Chem. Soc.*, 2012, **134**, 7874.
35 Y. Tang, L. Liu, H. Zhao, D. Jia and W. Liu, *J. Mater. Chem. A*, 2016, **4**, 2089.
36 L. Sun, W. Kong, H. Wu, Y. Wu, D. Wang, F. Zhao, K. Jiang, Q. Li, J. Wang and S. Fan, *Nanoscale*, 2016, **8**, 617.
37 A. Vinu, D. P. Sawant, K. Ariga, M. Hartmann and S. B. Halligudi, *Micropor. Mesopor. Mat.*, 2005, **80**, 195.
38 C. Jiang, E. Hosono, M. Ichihara, I. Honma and H. Zhou, *J. Electrochem. Soc.*, 2008, **155**, A553.
39 R. L. Penn and J. F. Banfield, *Science*, 1998, **281**, 969.
40 L. Shen, C. Yuan, H. Luo, X. Zhang, K. Xu and Y. Xia, *J. Mater. Chem.* 2010, **20**, 6998.
41 X. H. Yang, Z. Li, G. Liu, J. Xing, C. Sun, H. G. Yang and C. Li, *CrystEngComm*, 2011, **13**, 1378.
42 Q. Wang, J. Geng, C. Yuan, L. Kuai and B. Geng, *Electrochim. Acta*, 2016, **212**, 41.
43 L. Wu, X. Leng, Y. Liu, S. Wei, C. Li, G. Wang, J. Lian, Q. Jiang, A. Nie and T. Y. Zhang, *ACS Appl. Mater. Interfaces*, 2017, **9**, 4649.
44 T. F. Yi, Z. K. Fang, Y. Xie, Y. R. Zhu and S. Y. Yang, *ACS Appl.*

Mater. Interfaces, 2014, **6**, 20205.
45 S.-L. Chou, J.-Z. Wang, H.-K. Liu and S.-X. Dou, *J. Phys. Chem. C*, 2011, **115**, 16220.
46 H. Ge, L. Chen, W. Yuan, Y. Zhang, Q. Fan, H. Osgood, D. Matera, X.-M. Song and G. Wu, *J. Power Sources*, 2015, **297**, 436.
47 H. Ge, T. Hao, H. Osgood, B. Zhang, L. Chen, L. Cui, X. M. Song, O. Ogoke and G. Wu, *ACS Appl. Mater. Interfaces*, 2016, **8**, 9162.
48 Y. Shi, L. Wen, F. Li and H.-M. Cheng, *J. Power Sources*, 2011, **196**, 8610.
49 C. Lai, Y. Y. Dou, X. Li and X. P. Gao, *J. Power Sources*, 2010, **195**, 3676.
50 V. Augustyn, P. Simon and B. Dunn, *Energy Environ. Sci.*, 2014, **7**, 1597.
51 Z. Le, F. Liu, P. Nie, X. Li, X. Liu, Z. Bian, G. Chen, H. B. Wu and Y. Lu, *ACS Nano*, 2017, **11**, 2952.
52 J. Dong, Y. Jiang, Q. Li, Q. Wei, W. Yang, S. Tan, X. Xu, Q. An and L. Mai, *J. Mater. Chem. A*, 2017, **5**, 10827.
53 B. Wang, J. Wang, J. Cao, H. Ge and Y. Tang, *J. Power Sources*, 2014, **266**, 150.

Table of contents entry

Unique $Li_4Ti_5O_{12}/TiO_2$ multilayer arrays driven from substrate-free method demonstrate advanced surface lithium storage capability.